Nuclear Instruments and Methods in Physics Research A 1082 (2026) 171011

Contents lists available at ScienceDirect

Nuclear Inst. and Methods in Physics Research, A

journal homepage: www.elsevier.com/locate/nima

Full Length Article

Development of a simulation framework and experimental methods for understanding light collection in nanocomposite scintillators☆

Vojtech Zabloudil [a,c,*], Matteo Salomoni [a,b], Emanuele Mazzola [b,d], Luca Gironi [b,d], Sergio Brovelli [b,d], Solangel Rojas [c], Etiennette Auffray [a]

[a] European Organization for Nuclear Research (CERN), 1211 Geneva 23, Switzerland
[b] Department of Physics, University of Milano-Bicocca, 20126 Milano, Italy
[c] Czech Technical University in Prague, Jugoslávských Partyzánů 1580/3, 160 00, Prague, Czech Republic
[d] INFN–Sezione di Milano-Bicocca, 20126, Milan, Italy

ARTICLE INFO

Keywords:
Scintillator
Quantum dots
Nanocrystals
Nanocomposites
Monte Carlo simulations

ABSTRACT

The European Pathfinder project Unicorn aims to develop advanced nanoparticle-based scintillating materials for high-resolution and rapid-response radiation detection. This work explores the scintillation properties of nanocrystals in polymer matrices, aiming at applications in gamma and beta decay detection. The production of such scintillating composite requires to estimate the effect of absorption and scattering processes in the light transport on the performance of the final detector system. This contribution explores a novel experimental method using a spectrophotometer with a plug-in integrating sphere to obtain these parameters and investigates their influence on the light collection via Monte Carlo simulations in Geant4.

1. Introduction

Scintillators coupled with photodetectors are widely employed for detection of ionizing radiation in various fields such as high-energy physics, medical diagnostics, homeland security, and industry [1]. In research areas where large scintillator volumes are necessary, typically in the search for rare events, state-of-the-art inorganic crystals fall short in meeting the demands for cost and scalability while maintaining good energy resolution [2]. On the other hand, organic scintillators offer better scalability but suffer from limited energy resolution, highlighting the need for new materials specifically designed to meet these demanding requirements.

To address this, nanoparticle-based scintillators embedded in polymer or glass matrices offer a promising solution, providing compositional flexibility, scalability, and cost-effectiveness compared to conventional bulk crystals or commercial plastic scintillators [3–5]. Among their advantages over plastic scintillators is their potential to boast higher light yield, better energy resolution and faster scintillation decay featuring ultra-fast (subnanosecond) components [6]. Moreover, they emit in a narrower wavelength distribution.

However, modern nanocomposites face challenges due to their high scattering and absorption, which limit the amount of scintillation light reaching the photodetector and, consequently, their applicability in radiation detection [7]. To address this, it is essential to investigate how absorption and scattering properties affect the light transport and light collection at the photodetector to help manufacturers develop nanocomposites competitive with current scintillators on the market [8, 9].

2. Methods

2.1. Nanocomposite scintillators

To overcome the challenges of traditional scintillation materials such as inorganic crystals or organic plastic scintillators, an approach employing inorganic quantum confined nanocrystals (NCs) of nm dimensions embedded in polymer matrices might be exploited. This offers a combination of high density and good energy resolution of inorganics with the compositional flexibility and low production costs of plastic scintillators. Nanocomposites are an attractive prospect thanks to their efficient luminescence and excellent timing characteristics with effective decay times of a few nanoseconds [10–12]. This is also illustrated in Fig. 1 which presents the scintillation decay time spectrum of 0.1% CdSe/CdS dot-in-plate NCs in PMMA measured by TCSPC method under low-energy X-ray excitation using a set-up described in [13].

☆ This article is part of a Special issue entitled: 'VCI 2025' published in Nuclear Inst. and Methods in Physics Research, A.

* Corresponding author at: Czech Technical University in Prague, Jugoslávských Partyzánů 1580/3, 160 00, Prague, Czech Republic.
E-mail address: vojtech.zabloudil@cern.ch (V. Zabloudil).

https://doi.org/10.1016/j.nima.2025.171011
Received 20 April 2025; Received in revised form 4 September 2025; Accepted 10 September 2025
Available online 25 September 2025

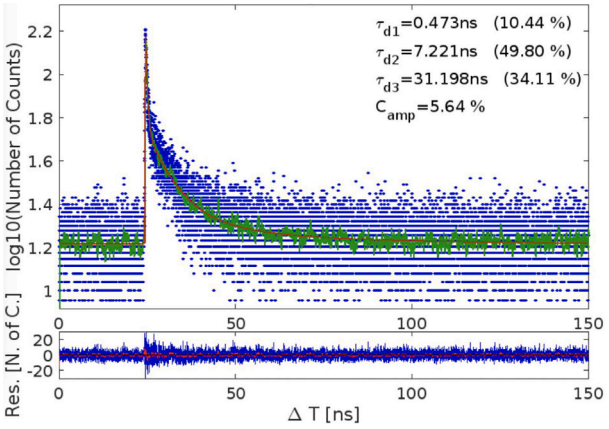

Fig. 1. Scintillation kinetics of 0.1% CdSe/CdS dot-in-plate NCs in PMMA measured by TCSPC method under X-ray excitation using a set-up described in [13].

Recently, nanocomposites have been successfully manufactured in high loadings (up to 40 wt%) thanks to co-polymerizable surface ligand exchange, thus increasing their stopping power for high energy X-rays or γ-ray while keeping a certain level of transparency [14].

2.2. Monte Carlo simulation

In order to study the effect of nanocomposite optical properties on the final detector performance, a Monte Carlo simulation framework modeling various geometries of the radiation detector using the GEANT4 toolkit was set up. As an example, a $5 \times 5 \times 5$ cm^3 block of a nanocomposite is simulated as a prospect for neutrinoless double beta decay detection [15]. The nanocomposite can be coupled to an arbitrary number of photodetectors; the two studied configurations were one photodetector coupled to one of the faces and six photodetectors, one on each face of the nanocomposite, surrounding the whole scintillator block. In the single-photodetector geometry, the remaining faces are covered with a perfectly reflective material to maximize light collection. An illustration of the geometries can be found in Fig. 2. A primary electron with a kinetic energy of 1.5 MeV, emulating one of the two electrons emitted during a neutrinoless double beta decay, is generated at random positions uniformly distributed within the volume and deposits its energy into the medium while producing optical photons by both scintillation and Cherenkov mechanisms. These are subsequently transported while undergoing absorption and scattering processes before being collected at the photocathode.

The described framework does not account for the effects of individual nanoparticles; instead, it treats the nanocomposite volume as homogeneous, using macroscopic properties that reflect the overall absorption and scattering of the nanocomposite.

2.3. Light transport in a scintillator

The transport of the scintillation photons is influenced by absorption and scattering processes that the photons undergo while traveling to the photodetector. During absorption, the photon is lost as a result of its interaction with the NCs; therefore lowering the efficiency of the scintillator. During scattering, which comprises Rayleigh and Mie components, the photon is elastically re-emitted in a different direction, effectively lengthening the photon path and causing the photon to be more likely absorbed by the NCs. This behavior is illustrated in subfigures (b), (c) and (d) of Fig. 2.

Rayleigh scattering occurs when the size of the scattering particle is much smaller than the incident photon wavelength. The angular distribution of re-emitted photons is almost isotropic while the scattering cross-section is heavily wavelength-dependent as $\sigma_{\text{Rayleigh}} \propto \lambda^{-4}$ [16].

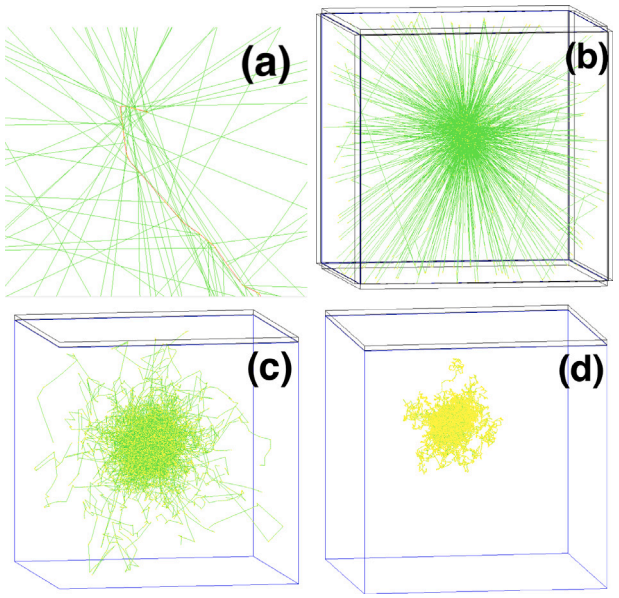

Fig. 2. Visualization of the trajectory (red line) of a 1.5 MeV electron producing scintillation and Cherenkov photons (green lines) (a). Scintillator nanocomposite with no scattering considered, read out with six photodetectors (black cuboids) (b). Nanocomposite read out with one photodetector only: both scattering attenuation lengths (Rayleigh and Mie) set to 1 mm (c), and to 0.1 mm (d). The yellow dots represent points of interaction with material.

Mie scattering is more significant when the wavelength of the incident photon is comparable to the size of the scattering particle [17]. The angular distribution of re-emitted photons is much more forward oriented while the cross-section is not heavily wavelength-dependent [18].

2.4. Light collection efficiency

To obtain the light collection efficiency at the photodetector, the simulation framework requires an input of the parameters describing the absorption properties and the scattering properties comprising of Rayleigh and Mie components.

The absorption properties are calculated from the experimental data of total transmittance of a 3-mm thick nanocomposite sample of 0.1% CdSe/CdS dot-in-plate NCs in PMMA (shown in Fig. 6). In this configuration, the losses due to scattering are minimal due to the small thickness of the sample; therefore, the absorption of the nanocomposite can be well estimated. The absorption length L_{abs} is obtained with the following equation

$$L_{\text{abs}} = \frac{1}{\alpha} = \left[A + 2\log(1-R)\right]\frac{\ln 10}{d}, \tag{1}$$

where α is the absorption coefficient, $A = \log(I/I_0)$ is the sample absorbance calculated from the transmittance $T = I/I_0$, $R = (n-1)^2/(n+1)^2$ is the sample reflectivity calculated using the refractive index n of PMMA only, and $d = 3$ mm is the sample thickness. Thanks to the correction using the sample reflectivity, Fresnel reflections on the surface are accounted for. The resulting dependence of the absorption length on wavelength is shown in Fig. 3.

The scattering attenuation lengths λ_{Ray} and λ_{Mie} are defined as the average length traveled by a photon before it is Rayleigh and Mie scattered, respectively. As these parameters are difficult to measure experimentally, the first step of our approach was to estimate the collection efficiency performing a scan over a range of anticipated scattering values of λ_{Ray} and λ_{Mie} while keeping the absorption fixed. The light collection efficiency (LCE), simply defined as

$$LCE = \frac{\#\text{ of ph reached photodetectors}}{\#\text{ of created ph (scintillation + Cherenkov)}}, \tag{2}$$

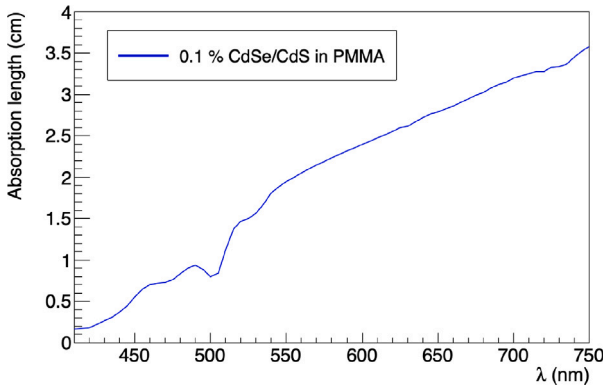

Fig. 3. Absorption length of a nanocomposite sample of 0.1% CdSe/CdS dot-in-plate NCs in PMMA calculated from its transmission properties.

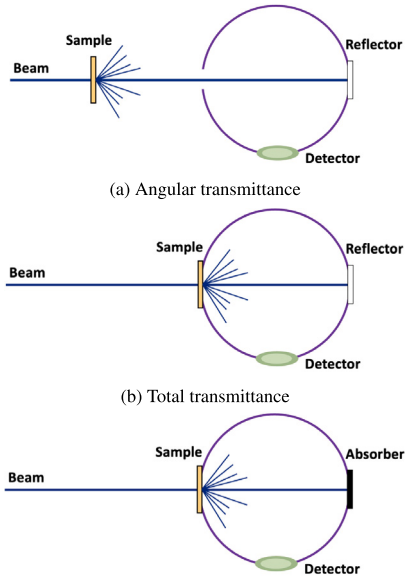

Fig. 4. Comparison of different configurations in the spectrophotometer set-up with a plug-in integrating sphere.

is then calculated for each of the different scattering attenuation lengths.

To estimate the LCE correctly, the refractive index of the nanocomposite was set equal to the refractive index of the polymer host (PMMA) while for the entrance window of the photodetector it was set to fused silica. The photodetector was coupled to the nanocomposite with optical grease ($n = 1.472$).

2.5. Experimental characterization of transmittance

In order to experimentally characterize the absorption and scattering properties of nanocomposites, a set-up comprised of a spectrophotometer with a plug-in integrating sphere, shown in Fig. 4, was designed. The set-up offers the versatility to exchange between three different configurations focusing on the collection of transmitted light through the sample.

The angular transmittance configuration collects the light transmitted through the sample while the part that was scattered is lost due to the large distance between the sample and the entrance window of the integrating sphere.

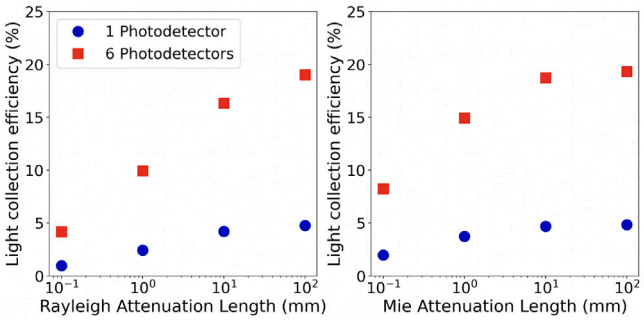

Fig. 5. Simulation studies of the light collection efficiency dependence on λ_{Ray} while keeping $\lambda_{\mathrm{Mie}} = 10^9$ mm (left) and the dependence on λ_{Mie} while keeping $\lambda_{\mathrm{Ray}} = 10^9$ mm (right) for a $5 \times 5 \times 5$ cm^3 nanocomposite of CdSe/CdS dot-in-plate NCs in PMMA matrix coupled to 1 and 6 photodetectors depicted by blue circles and red squares, respectively.

The total transmittance configuration where the sample is placed at the entrance window uses a reflective plate at the other end of the integrating sphere which allows to recollect the transmitted part of the light as well as the part of the light that is scattered in the direction of the integrating sphere. For a thin enough sample, this configuration provides the best reference of solely absorption properties of the measured sample.

Finally, the diffuse transmittance configuration uses the same sample placement as in total configuration, but the reflector at the end of the integrating sphere is exchanged for an absorber. In this way, the light that is only transmitted through the sample will be absorbed, while the scattered part will be recollected.

3. Results and discussion

3.1. Light collection efficiency scan

In order to study the effect of different scattering components on the light collection efficiency, 100 k events were generated per each scattering length value and the LCE was calculated according to (2). For all of the simulation runs, the absorption properties of the nanocomposite were fixed using the experimental data as discussed above. The developed framework allows to vary λ_{Ray} while keeping λ_{Mie} fixed, and vice versa to see the individual effects of both scattering components on the LCE. The results are summarized in Fig. 5.

The simulation results indicate that the current level of NC absorption significantly limits the feasibility of using a $5 \times 5 \times 5$ cm^3 nanocomposite with a single photodetector. Even in the absence of scattering and with perfectly reflective material covering the remaining faces, the light collection efficiency (LCE) is around 5%. However, surrounding the nanocomposite cube with six photodetectors, which would largely complicate the detector design, increases the LCE to approximately 20% under the same conditions. Nevertheless, as scattering length values approach realistic levels, the LCE rapidly declines. Notably, Rayleigh scattering has a more severe impact than Mie scattering due to differences in the angular distribution of re-emitted photons after scattering.

The simulation framework can be easily generalized for different energies and species of the primary particle, making it possible to perform a comprehensive study of using a nanocomposite as a radiation detector.

3.2. Experimental transmission studies

The experimental method for studying the nanocomposite absorption and scattering properties was tested using a sample of CdSe/CdS

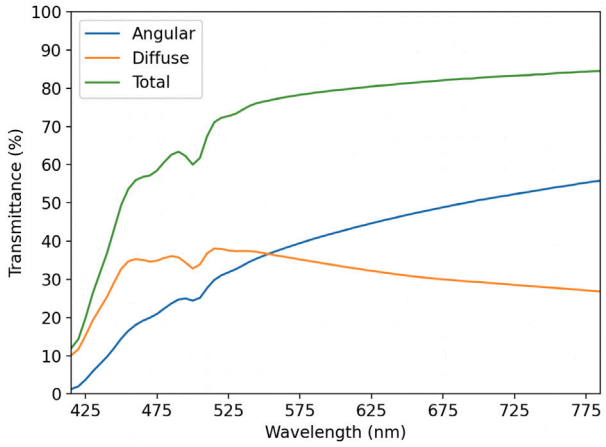

Fig. 6. Transmittance of a 3-mm thick nanocomposite sample of 0.1% CdSe/CdS dot-in-plate NCs in PMMA measured by the spectrophotometer set-up with a plug-in integrating sphere in three configurations.

dot-in-plate NCs in a PMMA matrix. The results of the three measurements are summarized in Fig. 6. As observed, the total transmittance, represented by the green line, remains below the 90% limit event at longer wavelengths, indicating the presence of absorption. For wavelengths below 550 nm, transmittance drops sharply, highlighting strong NC absorption in this region (peaks of the nanocomposite excitation and emission spectra are around 370–410 nm and 505 nm, respectively). Additionally, the diffuse transmittance curve, shown in orange, deviates significantly from the expected Rayleigh scattering trend, suggesting a strong contribution from the Mie component.

It is pivotal to complement the experimental measurements with additional GEANT4 simulations of material transmittance in order to decouple the two scattering components and extract their attenuation lengths. Similarly, the method will largely benefit from measurements of nanocomposites with fixed NC concentration and varying thickness, and vice versa.

Once the experimental method to determine the scattering lengths is validated, different nanocomposite samples can be characterized. The output of this method can be used as an input for the simulation of the LCE to simulate nanocomposites of different sizes, geometries and read-out techniques and to evaluate their feasibility as radiation detectors.

4. Conclusion

This study presents a newly developed simulation framework for investigating the effects of scattering and absorption on light transport and collection in nanocomposite scintillators. The first evaluation with a nanocomposite of CdSe/CdS dot-in-plate nanocrystals in PMMA demonstrates that the current absorption levels of nanocrystals (NCs) significantly limit the light collection efficiency (LCE) even under the idealized assumption of no scattering. This limitation is particularly evident in simple experimental configurations involving a single photodetector coupled to one face of the nanocomposite, with the remaining faces covered by a reflector. While surrounding the nanocomposite with multiple photodetectors enhances the LCE, this approach complicates the detector design and may be impractical. Furthermore, as scattering is introduced in the simulation with attenuation length values approaching realistic conditions, the LCE declines sharply, with Rayleigh scattering having a more detrimental effect than Mie scattering due to its nearly isotropic photon redistribution.

In parallel, an experimental method using a spectrophotometer with an integrating sphere was developed to validate the simulation results and serve as a tool for characterization of the absorption and scattering of nanocomposites. Preliminary results support the validity of this approach, paving the way for comprehensive characterization of various nanocomposite samples and their subsequent optimization for radiation detection. Future work will focus on refining nanocomposite formulations to minimize absorption and scattering losses, e.g., by identifying polymer matrices with refractive indices that best match those of the nanocrystals. This approach aims to enhance the competitiveness of nanocomposites with existing scintillators and address their current limitations in specific applications.

Declaration of competing interest

The authors declare the following financial interests/personal relationships which may be considered as potential competing interests: Vojtech Zabloudil reports financial support was provided by European Innovation Council. If there are other authors, they declare that they have no known competing financial interests or personal relationships that could have appeared to influence the work reported in this paper.

Acknowledgments

This work is performed in the framework of the European Pathfinder Open Horizon Europe project UNICORN (GA 101098649) and the Crystal Clear Collaboration, it received support from the Grant Agency of the Czech Technical University in Prague, Grant Number SGS24/145/OHK4/3T/14. The authors would like to thank Thomas Schneider for the access to the spectrophotometer. During the preparation of this work the authors used ChatGPT in order to clarify and refine the content of the article. After using this tool, the authors reviewed and edited the content as needed and take full responsibility for the content of the publication.

References

[1] M. Nikl, et al., Recent R & D trends in inorganic single-crystal scintillator materials for radiation detection, Adv. Opt. Mater. 3 (2015) 463–481, http://dx.doi.org/10.1002/adom.201400571.

[2] C. Dujardin, et al., Needs, Trends, and Advances in Inorganic Scintillators, IEEE Trans. Nucl. Sci. 65 (8) (2018) 1977–1997, http://dx.doi.org/10.1109/TNS.2018.2840160.

[3] C. Dujardin, et al., Inorganic nanoscintillators: Current trends and future perspectives, Adv. Opt. Mater. (2025) 2402739, http://dx.doi.org/10.1002/adom.202402739.

[4] A. Anand, et al., Advances in perovskite nanocrystals and nanocomposites for scintillation applications, ACS Energy Lett. 9 (3) (2024) 1261–1287, http://dx.doi.org/10.1021/acsenergylett.3c02763, arXiv:2406.13325.

[5] V. Vaněček, et al., Advanced Halide Scintillators: From the Bulk to Nano, Adv. Photonics Res. 3 (8) (2022) 2200011, http://dx.doi.org/10.1002/adpr.202200011.

[6] R.M. Turtos, et al., On the use of CdSe scintillating nanoplatelets as time taggers for high-energy gamma detection, Npj 2D Mater. Appl. 3 (1) (2019) 37, http://dx.doi.org/10.1038/s41699-019-0120-8.

[7] P. Singh, et al., Bright innovations: Review of next-generation advances in scintillator engineering, ACS Nano 18 (22) (2024) 14029–14049, http://dx.doi.org/10.1021/acsnano.3c12381.

[8] J.K. Wilson, et al., Optimisation of monolithic nanocomposite and transparent ceramic scintillation detectors for positron emission tomography, Sci. Rep. 10 (1) (2020) 1409, http://dx.doi.org/10.1038/s41598-020-58208-y.

[9] M.C. Tan, et al., Transparent infrared-emitting CeF_3 :Yb-Er Polymer Nanocomposites for optical applications, ACS Appl. Mater. Interfaces 2 (7) (2010) 1884–1891, http://dx.doi.org/10.1021/am100228j.

[10] R.M. Turtos, et al., Towards a metamaterial approach for fast timing in PET: Experimental proof-of-concept, Phys. Med. Biology 64 (18) (2019) 185018, http://dx.doi.org/10.1088/1361-6560/ab18b3.

[11] G. Konstantinou, et al., Metascintillators for Ultrafast Gamma Detectors: A Review of Current State and Future Perspectives, IEEE Trans. Radiat. Plasma Med. Sci. 6 (1) (2022) 5–15, http://dx.doi.org/10.1109/TRPMS.2021.3069624.

[12] K. Děcká, et al., Timing performance of lead halide perovskite nanoscintillators embedded in a polystyrene matrix, J. Mater. Chem. C 10 (35) (2022) 12836–12843, http://dx.doi.org/10.1039/D2TC02060B.

[13] F. Pagano, et al., A new method to characterize low stopping power and ultrafast scintillators using pulsed x-rays, Front. Phys. 10 (2022) http://dx.doi.org/10.3389/fphy.2022.1021787.

[14] J. Král, et al., Towards high loading cesium lead halide nanocomposites for radiation detection, J. Phys.: Mater. 8 (1) (2024) 015007, http://dx.doi.org/10.1088/2515-7639/ad9e2f.

[15] M.J. Dolinski, et al., Neutrinoless Double-Beta Decay: Status and Prospects, Annu. Rev. Nucl. Part. Sci. 69 (1) (2019) 219–251, http://dx.doi.org/10.1146/annurev-nucl-101918-023407.

[16] C.F. Bohren, et al., Absorption and Scattering of Light By Small Particles, A Wiley-Interscience Publication, Wiley-CH Verlag GmbH & Co KGaA, New York, 2004, http://dx.doi.org/10.1002/9783527618156.

[17] J. Shen, et al., Light Scattering in nanoparticle doped transparent polyimide substrates, ACS Appl. Mater. Interfaces 9 (17) (2017) 14990–14997, http://dx.doi.org/10.1021/acsami.7b03070.

[18] J.D. Lockwood, Rayleigh and mie scattering, in: R. Luo (Ed.), Encyclopedia of Color Science and Technology, Springer Berlin Heidelberg, Berlin, Heidelberg, 2015, pp. 1–12, http://dx.doi.org/10.1007/978-3-642-27851-8_218-1.